On the Design of Frequency-Invariant Beampatterns With Uniform Circular Microphone Arrays

Gongping Huang, *Student Member, IEEE*, Jacob Benesty, and Jingdong Chen, *Senior Member, IEEE*

***Abstract*—This paper deals with two critical issues about uniform circular arrays (UCAs): frequency-invariant response and steering flexibility. It focuses on some optimal design of frequency-invariant beampatterns in any desired direction along the sensor plane. The major contributions are as follows. 1) We explain how to include the steering information in the desired directivity pattern. 2) We show that the optimal approximation of the beamformer's beampattern with a UCA from a least-squares error perspective is the Jacobi–Anger expansion. 3) We develop an approach to the design of any desired symmetric directivity pattern, where the deduced beampattern is almost frequency invariant and its main beam can be pointed to any wanted direction in the sensor plane. 4) With the proposed approach, we derive an explicit form of the white noise gain (WNG) and the directivity factor (DF), and explain clearly the white noise amplification problem at low frequencies and the DF degradation at high frequencies. The analysis also indicates that increasing the number of microphones can always improve the WNG. We show that the proposed method is a generalization of circular differential microphone arrays. The relationship between the proposed method and the so-called circular harmonics beamformers is also discussed.**

***Index Terms*—Microphone arrays, uniform circular arrays, beampattern design, frequency-invariant beampattern, steering, fixed beamforming, white noise gain, directivity factor.**

I. Introduction

MICROPHONE array beamforming, which aims at recovering a signal of interest from noisy observations with a spatial filter, has been widely used in voice communications and human-machine interfaces. Much attention has been paid to this area and many interesting techniques have been developed in the literature [1]–[21]. One of the most popular algorithms is the delay-and-sum (DS) beamforming [7], [8]. However, the response of this beamformer is frequency dependent, and its beamwidth is inversely proportional to the frequency, so the DS beamformer is not effective in dealing with low-frequency noise and interference. Moreover, the noise is not uniformly attenuated over its entire spectrum, which results in some disturbing artifacts at the array output [10]. To deal with these problems, many broadband beamforming techniques, such as nested arrays [11], narrowband decomposition beamforming [12], differential beamforming [13]–[16], and modal beamforming [17]–[27], have been developed over the last few decades.

Among those, differential beamforming with small and compact apertures has attracted much research interest since it can form frequency-invariant beampatterns, and has the potential to attain high directional gains [13]–[15], [28]. Conventional design of differential microphone arrays (DMAs) lacks flexibility in forming different patterns and suffers from serious white noise amplification [2], [29], making it very challenging to implement DMAs in practical systems. A new approach to differential beamforming was developed recently [10], which can overcome the aforementioned drawbacks. In this method, linear DMAs (LDMAs) are designed in the short-time Fourier transform (STFT) domain with some null constraints from the desired directivity pattern. However, LDMAs do not have much flexibility in terms of beam steering; the maximum flexibility of designing different directivity pattens and optimal performance in terms of DF occur only at the angles 0° and 180° [2], [10]. This is why in the design of LDMAs, we always assume that the desired source signal propagates from the endfire directions [10]. In applications where beam steering is needed, one may consider to use circular arrays, which have much better steering capabilities [30]–[32].

Differential beamforming with circular microphone arrays have been studied in [30], where spatial filters are obtained by solving some linear systems of equations determined by null constraints from the desired directivity pattern. With a uniform circular array (UCA) consisting of M microphones, a differential beamformer is guarantied to perfectly steer to M different directions, i.e., the M angular positions of the array elements. However, theory is still lacking on how to steer the beampattern of a circular differential microphone array (CDMA) to any direction. Another widely used technique to design frequency-invariant beamformers is the circular harmonics beamformers (CHBs) [17]–[19]. Generally, CHBs are based on

Manuscript received November 10, 2016; revised February 26, 2017; accepted March 24, 2017. Date of publication March 30, 2017; date of current version April 24, 2017. This work was supported in part by the NSFC Distinguished Young Scientists Fund under Grant 61425005. The work of G. Huang was supported in part by the China Scholarship Council. The associate editor coordinating the review of this manuscript and approving it for publication was Dr. Christian Hendriks. *(Corresponding author: Jingdong Chen.)*

G. Huang is with the Center of Intelligent Acoustics and Immersive Communications, and School of Marine Science and Technology, Northwestern Polytechnical University, Xi'an, Shaanxi 710072, China, and also with the Institut National de la Recherche Scientifique-Énergie, Matériaux et Télécommunications, University of Quebec, Montreal, QC H5A 1K6, Canada (e-mail: gongpinghuang@gmail.com).

J. Benesty is with Institut National de la Recherche Scientifique-Énergie, Matériaux et Télécommunications (INRS-EMT), University of Quebec, Montreal, QC H5A 1K6, Canada (e-mail: benesty@emt.inrs.ca).

J. Chen is with the Center of Intelligent Acoustics and Immersive Communications, Northwestern Polytechnical University, Xi'an, Shaanxi 710072, China (e-mail: jingdongchen@ieee.org).

Color versions of one or more of the figures in this paper are available online at http://ieeexplore.ieee.org.

Digital Object Identifier 10.1109/TASLP.2017.2689681

decomposing the sound field into a series of circular harmonics, and the beamforming output is then obtained by combining circular harmonics with appropriate weighting coefficients. However, there are still many important questions to be answered with CHBs, such as how to design CHBs in a more flexible way, i.e., with any desired symmetric directivity pattern, what is the connection between CDMAs and CHBs, etc.

This paper attempts to answer the aforementioned questions and presents new insights into the design of frequency-invariant beampatterns with UCAs. The major contributions are as follows. First, we explain how to include the steering information in the desired directivity pattern. Second, we show that the optimal approximation of the beamformer beampattern with a UCA from a least-squares error (LSE) perspective is the Jacobi-Anger expansion. Third, based on this approximation, we develop a new approach to the design of any desired symmetric directivity pattern, where the deduced beampattern is almost frequency invariant and its main beam can be pointed at any look direction in the sensor plane. Fourth, with the proposed approach, we derive an explicit form of the white noise gain (WNG) and the directivity factor (DF), and explain the white noise amplification problem at low frequencies and the DF degradation at high frequencies. Our analysis also shows that increasing the number of microphones can always improve the WNG. Finally, we show the relation of the proposed approach with CDMAs and CHBs.

The remainder of this paper is organized as follows. Section II presents the signal model, problem formulation, and performance measures. Section III describes two fundamental ways to illustrate the desired symmetric directivity pattern. Section IV discusses how to optimally approximate the beamformer beampattern and design frequency-invariant beamformers from any desired symmetric directivity pattern. Section V presents some simulation results to validate the theoretical derivations. Finally, some conclusions are given in Section VI.

II. Signal Model, Problem Formulation, and Performance Measures

In this study, we consider a farfield source signal (plane wave), that propagates in an anechoic acoustic environment at the speed of sound, i.e., $c = 340$ m/s, and impinges on a UCA composed of M omnidirectional microphones with radius r. Without loss of generality, we assume that all the sensors are in the horizonal plane, the center of the UCA coincides with the origin of the Cartesian coordinate system, the direction of the source signal to the array is parameterized by the azimuth angle θ, the azimuth angles are measured anti-clockwise from the x axis, i.e., at $\theta = 0$, and sensor 1 of the array is placed on the x axis, i.e., at $\theta = 0$. In this scenario, the steering vector of length M is [33], [34]

$$\mathbf{d}(\omega,\theta) = \left[e^{\jmath\varpi\cos(\theta-\psi_1)} \quad \cdots \quad e^{\jmath\varpi\cos(\theta-\psi_M)} \right]^T, \tag{1}$$

where the superscript ^{T} is the transpose operator, $\jmath$ is the imaginary unit with $\jmath^2 = -1$, $\varpi = \omega r/c$, $\omega = 2\pi f$ is the angular frequency, $f > 0$ is the temporal frequency, and

$$\psi_m = \frac{2\pi(m-1)}{M} \tag{2}$$

is the angular position of the mth array element. The acoustic wavelength is $\lambda = c/f$ and, for a UCA, the interelement spacing is

$$\delta = 2r\sin\left(\frac{\pi}{M}\right). \tag{3}$$

In order to avoid spatial aliasing, which has the negative effect of generating grating lobes (i.e., copies of the main lobe, which usually points toward the desired signal), it is assumed that $\delta \leq \lambda/2$ [10], [30], [35]. From the approximation $\delta \approx 2\pi r/M$, an equivalent manner to express the previous condition is

$$\varpi \leq \frac{M}{2}. \tag{4}$$

Consider the general case where the desired signal comes from the direction θ_{s} and the corresponding propagation vector is $\mathbf{d}(\omega,\theta_{\mathrm{s}})$. Then, our objective is to design a beampattern from a desired directivity pattern whose main beam points in the direction θ_{s} and, at the same time, is frequency invariant. For that, a complex weight, $H_m^*(\omega)$, $m = 1, 2, \ldots, M$, is applied to the output of the mth sensor, where the superscript * denotes complex conjugation. The weighted outputs are then summed together to form the fixed beamformer output. Putting all the gains together in a vector of length M, we get

$$\mathbf{h}(\omega) = \left[H_1(\omega) \quad H_2(\omega) \quad \cdots \quad H_M(\omega) \right]^T. \tag{5}$$

Sometimes the distortionless constraint in the desired look direction is needed, i.e.,

$$\mathbf{h}^H(\omega)\,\mathbf{d}(\omega,\theta_{\mathrm{s}}) = 1, \tag{6}$$

where the superscript ^{H} is the conjugate-transpose operator.

The three most important performance measures to evaluate how the fixed beamformer, $\mathbf{h}(\omega)$, performs are the beampattern, the directivity factor (DF), and the white noise gain (WNG).

The beampattern describes the sensitivity of the fixed beamformer to a plane wave impinging on the UCA from the direction θ. Mathematically, it is defined as

$$\begin{aligned}\mathcal{B}[\mathbf{h}(\omega),\theta] &= \mathbf{h}^H(\omega)\,\mathbf{d}(\omega,\theta) \\ &= \sum_{m=1}^{M} H_m^*(\omega) e^{\jmath\varpi\cos(\theta-\psi_m)}.\end{aligned} \tag{7}$$

So, for a well designed filter, $\mathbf{h}(\omega)$, $|\mathcal{B}[\mathbf{h}(\omega),\theta_{\mathrm{s}}]|^2$ should be maximal at $\theta = \theta_{\mathrm{s}}$ and $|\mathcal{B}[\mathbf{h}(\omega),\theta]|^2 < |\mathcal{B}[\mathbf{h}(\omega),\theta_{\mathrm{s}}]|^2$ for $\theta \neq \theta_{\mathrm{s}}$.

Given a beampattern $\mathcal{B}[\mathbf{h}(\omega),\theta]$, the DF quantifies its directional property, which in turn tells the ability of the beamformer in suppressing spatial noise from directions other than the look direction. The DF is defined as the ratio between the magnitude squared beampattern in the desired look direction and the averaged magnitude squared beampattern over the entire

space [30], [36]. With our signal model, the DF is given by

$$\mathcal{D}\left[\mathbf{h}\left(\omega\right)\right]=\frac{\left|\mathbf{h}^{H}\left(\omega\right)\mathbf{d}\left(\omega,\theta_{\mathrm{s}}\right)\right|^{2}}{\mathbf{h}^{H}\left(\omega\right)\mathbf{\Gamma}_{\mathrm{d}}\left(\omega\right)\mathbf{h}\left(\omega\right)}, \tag{8}$$

where the elements of the $M\times M$ matrix $\mathbf{\Gamma}_{\mathrm{d}}\left(\omega\right)$ are given by

$$\left[\mathbf{\Gamma}_{\mathrm{d}}\left(\omega\right)\right]_{ij}=\mathrm{sinc}\left(\frac{\omega\delta_{ij}}{c}\right), \tag{9}$$

with $i,j=1,2,\ldots,M$,

$$\mathrm{sinc}(x)=\frac{\sin x}{x}, \tag{10}$$

and

$$\delta_{ij}=2r\left|\sin\left[\frac{\pi\left(i-j\right)}{M}\right]\right| \tag{11}$$

being the distance between sensors i and j. It can be shown that $\mathbf{\Gamma}_{\mathrm{d}}\left(\omega\right)$ is a circulant matrix. Obviously, $\mathcal{D}\left[\mathbf{h}\left(\omega\right)\right]\leq\mathbf{d}^{H}\left(\omega,\theta_{\mathrm{s}}\right)\mathbf{\Gamma}_{\mathrm{d}}^{-1}\left(\omega\right)\mathbf{d}\left(\omega,\theta_{\mathrm{s}}\right),\ \forall\mathbf{h}\left(\omega\right)$.

An array is far to be perfect; not only its sensors contain self noise, mismatch among sensors is also unavoidable. These imperfections may also affect the performance of the beamformer and the degree of the impact depends on the level of the imperfection as well as the beamforming algorithm. An effective measure that evaluates the performance of a beamformer in the presence of array imperfection as well as other uncertainties is the so-called WNG [37], which is defined as

$$\mathcal{W}\left[\mathbf{h}\left(\omega\right)\right]=\frac{\left|\mathbf{h}^{H}\left(\omega\right)\mathbf{d}\left(\omega,\theta_{\mathrm{s}}\right)\right|^{2}}{\mathbf{h}^{H}\left(\omega\right)\mathbf{h}\left(\omega\right)}. \tag{12}$$

It can be verified that $\mathcal{W}\left[\mathbf{h}\left(\omega\right)\right]\leq M,\ \forall\mathbf{h}\left(\omega\right)$.

III. Desired Directivity Pattern

It is well known that any desired symmetric directivity pattern whose main beam points in the direction $\theta=0$ has the form [38]:

$$\begin{aligned}\mathcal{B}\left(\mathbf{a}_{N},\theta\right)&=\sum_{n=0}^{N}a_{N,n}\cos\left(n\theta\right)\\&=\mathbf{a}_{N}^{T}\mathbf{p}_{\mathrm{c}}\left(\theta\right),\end{aligned} \tag{13}$$

where $a_{N,n},\ n=0,1,\ldots,N$, are real coefficients, N is called the order of the beampattern, and

$$\begin{aligned}\mathbf{a}_{N}&=\left[\begin{array}{cccc}a_{N,0}&a_{N,1}&\cdots&a_{N,N}\end{array}\right]^{T},\\\mathbf{p}_{\mathrm{c}}\left(\theta\right)&=\left[\begin{array}{cccc}1&\cos\theta&\cdots&\cos\left(N\theta\right)\end{array}\right]^{T}.\end{aligned}$$

The values of the coefficients $a_{N,n},\ n=0,1,\ldots,N$ determine the shape of the directivity pattern. (The reader is referred to [30] for the values of the coefficients of widely used directivity patterns such as the dipole, the cardioid, the supercardioid, and the hypercardioid.) It may be convenient to use a normalization convention for these coefficients. For that, in the direction of the main beam, i.e., $\theta=0$, we would like the directivity pattern to be equal to 1, i.e., $\mathcal{B}\left(\mathbf{a}_{N},0\right)=1$. Therefore, we have

$$\sum_{n=0}^{N}a_{N,n}=1. \tag{14}$$

As a result, we may choose the first coefficient as

$$a_{N,0}=1-\sum_{n=1}^{N}a_{N,n}. \tag{15}$$

Since $\cos\theta$ is an even function, so is $\mathcal{B}\left(\mathbf{a}_{N},\theta\right)$. Therefore, on a polar plot, $\mathcal{B}\left(\mathbf{a}_{N},\theta\right)$ is symmetric about the axis $0\leftrightarrow\pi$ and we can limit its study to $\theta\in[0,\pi]$.

With the ideal form of the beampattern given in (13), the problem of beamforming becomes one of finding the beamforming filter, $\mathbf{h}\left(\omega\right)$, such that the designed beampattern, $\mathcal{B}\left[\mathbf{h}\left(\omega\right),\theta\right]$, approaches the target beampattern, $\mathcal{B}\left(\mathbf{a}_{N},\theta\right)$, that is specified by the set of coefficients $a_{N,n},\ n=0,1,\ldots,N$. This can be done using the method developed in [30], where the filter is obtained from the solution of a linear system constructed from the null information of $\mathcal{B}\left(\mathbf{a}_{N},\theta\right)$. However, the designed beamformer can only be steered to M directions (without any beampattern deformation) where the M sensors are located. Another way to determine this filter is by solving a linear system constructed by approximating the beampattern with the Jacobi-Anger series expansions. However, this method does not improve the steering ability, i.e., perfect steering is still limited to the M directions.

In this paper, we attempt to generalize the method in [30] to design frequency-invariant beampatterns with UCAs, which can be steered to any directions in the plane in which the sensors are located. Let θ_{s} be the steering angle, the directivity pattern:

$$\mathcal{B}\left(\mathbf{a}_{N},\theta-\theta_{\mathrm{s}}\right)=\mathbf{a}_{N}^{T}\mathbf{p}_{\mathrm{c}}\left(\theta-\theta_{\mathrm{s}}\right), \tag{16}$$

is a simple version of $\mathcal{B}\left(\mathbf{a}_{N},\theta\right)$ rotated by the angle θ_{s}; so now the main beam of (16) points in the direction θ_{s} and $\mathcal{B}\left(\mathbf{a}_{N},\theta-\theta_{\mathrm{s}}\right)$ is symmetric about the axis $\theta_{\mathrm{s}}\leftrightarrow\theta_{\mathrm{s}}+\pi$, with $\theta\in[\theta_{\mathrm{s}},\theta_{\mathrm{s}}+\pi]$.

The formulation in (13) is often associated with linear arrays. However, for two-dimensional arrays where steering is important, (13) or (16) may not be complete. Another interesting and fundamental way to write (13) when the steering is part of the design of the beampatterns is

$$\begin{aligned}\mathcal{B}\left(\mathbf{a}_{N},\theta\right)&=\frac{1}{2}\sum_{n=0}^{N}a_{N,n}\left(e^{\jmath n\theta}+e^{-\jmath n\theta}\right)\\&=a_{N,0}+\frac{1}{2}\sum_{i=1}^{N}a_{N,i}e^{\jmath i\theta}+\frac{1}{2}\sum_{i=-N}^{-1}a_{N,-i}e^{\jmath i\theta}\\&=\sum_{n=-N}^{N}b_{2N,n}e^{\jmath n\theta}\\&=\sum_{n=-N}^{N}b_{2N,n}e^{-\jmath n\theta}\\&=\mathbf{b}_{2N}^{T}\mathbf{p}_{e}\left(\theta\right)\\&=\mathcal{B}\left(\mathbf{b}_{2N},\theta\right),\end{aligned} \tag{17}$$

where

$$\begin{cases} b_{2N,0} = a_{N,0} \\ b_{2N,i} = b_{2N,-i} = \dfrac{1}{2} a_{N,i},\ i = 1, 2, \ldots, N \end{cases} \tag{18}$$

and

$$\mathbf{b}_{2N} = \begin{bmatrix} b_{2N,-N} & \cdots & b_{2N,0} & \cdots & b_{2N,N} \end{bmatrix}^T,$$
$$\mathbf{p}_e(\theta) = \begin{bmatrix} e^{-\jmath N\theta} & \cdots & 1 & \cdots & e^{\jmath N\theta} \end{bmatrix}^T.$$

The vector $\mathbf{p}_e(\theta)$ of length $2N+1$ is composed of circular harmonics of different orders. At the steering angle θ_{s}, we have

$$\begin{aligned} \mathcal{B}(\mathbf{b}_{2N}, \theta - \theta_{\mathrm{s}}) &= \mathbf{b}_{2N}^T \mathbf{p}_e(\theta - \theta_{\mathrm{s}}) \\ &= \left[\boldsymbol{\Upsilon}(\theta_{\mathrm{s}})\, \mathbf{b}_{2N}\right]^T \mathbf{p}_e(\theta) \\ &= \mathbf{c}_{2N}^T(\theta_{\mathrm{s}})\, \mathbf{p}_e(\theta) \\ &= \mathcal{B}[\mathbf{c}_{2N}(\theta_{\mathrm{s}}), \theta], \end{aligned} \tag{19}$$

where

$$\boldsymbol{\Upsilon}(\theta_{\mathrm{s}}) = \mathrm{diag}\left(e^{\jmath N\theta_{\mathrm{s}}}, \ldots, 1, \ldots, e^{-\jmath N\theta_{\mathrm{s}}}\right) \tag{20}$$

is a diagonal matrix and

$$\begin{aligned} &\mathbf{c}_{2N}(\theta_{\mathrm{s}}) \\ &= \begin{bmatrix} c_{2N,-N}(\theta_{\mathrm{s}}) & \cdots & c_{2N,0}(\theta_{\mathrm{s}}) & \cdots & c_{2N,N}(\theta_{\mathrm{s}}) \end{bmatrix}^T \\ &= \boldsymbol{\Upsilon}(\theta_{\mathrm{s}})\, \mathbf{b}_{2N}. \end{aligned} \tag{21}$$

This shows that a rotation of the directivity pattern corresponds to a simple modification of its coefficients. In other words, these new coefficients [which are the components of $\mathbf{c}_{2N}(\theta_{\mathrm{s}})$] not only determine the shape of the directivity pattern but also the direction of the main beam. This comes at a price: the number of coefficients is now equal to $2N+1$ instead of N when steering is not taken into account. This time $\theta \in [0, 2\pi]$. Therefore, our desired directivity pattern is $\mathcal{B}[\mathbf{c}_{2N}(\theta_{\mathrm{s}}), \theta]$. In practice, the shape of the beampattern is determined by $\mathbf{a}_N$ (which is given by design) and the steering by θ_{s}; then, $\mathbf{b}_{2N}$ is obtained from (18) and $\mathbf{c}_{2N}(\theta_{\mathrm{s}})$ from (21). The normalization convention on $\mathbf{a}_N$, which will always be used here, implies that $\mathcal{B}[\mathbf{c}_{2N}(\theta_{\mathrm{s}}), \theta_{\mathrm{s}}] = 1$.

IV. Beampattern Design

In this section, we first give an alternative expression of the beamformer beampattern and show how to optimally approximate it. From this approximation, we then show how to design any desired symmetric directivity pattern. The deduced beampattern is almost frequency invariant and its main beam can be pointed at any desired direction.

A. Optimal Approximation of the Beamformer Beampattern

In order to be able to design any desired directivity pattern, $\mathcal{B}[\mathbf{c}_{2N}(\theta_{\mathrm{s}}), \theta]$, with $\mathcal{B}[\mathbf{h}(\omega), \theta]$, where $\mathbf{h}(\omega)$ has to be derived accordingly, we need to approximate the exponential function that appears in (7) in terms of circular harmonics since $\mathcal{B}[\mathbf{c}_{2N}(\theta_{\mathrm{s}}), \theta]$ is also a decomposition of these harmonics. Since the complex-valued exponential function is infinitely differentiable with respect to the variable θ, we can find the complex-valued coefficients $s_n,\ n = 0, \pm 1, \pm 2, \ldots$ such that [38]

$$e^{\jmath\varpi\cos(\theta-\psi_m)} = \lim_{N\to\infty} \sum_{n=-N}^{N} s_n e^{-\jmath n\theta}. \tag{22}$$

By limiting the above series to a fixed order of N, we obtain the corresponding partial sum. Now, we propose to find the coefficients $s_n,\ n = 0, \pm 1, \ldots, \pm N$ in the best possible way in a least-squares error (LSE) sense, i.e., by minimizing the criterion [39]:

$$\begin{aligned} &\mathrm{LSE}(\mathbf{s}_{2N}) \\ &= \frac{1}{2\pi} \int_0^{2\pi} \left| e^{-\jmath\varpi\cos(\theta-\psi_m)} - \sum_{n=-N}^{N} s_n^* e^{\jmath n\theta} \right|^2 d\theta \\ &= \frac{1}{2\pi} \int_0^{2\pi} \left| e^{-\jmath\varpi\cos(\theta-\psi_m)} - \mathbf{s}_{2N}^H \mathbf{p}_e(\theta) \right|^2 d\theta \\ &= 1 - \mathbf{v}_e^H(\jmath\varpi\psi_m)\, \mathbf{s}_{2N} - \mathbf{s}_{2N}^H \mathbf{v}_e(\jmath\varpi\psi_m) \\ &\quad + \mathbf{s}_{2N}^H \mathbf{M}_e \mathbf{s}_{2N}, \end{aligned} \tag{23}$$

where

$$\mathbf{s}_{2N} = \begin{bmatrix} s_{-N} & \cdots & s_0 & \cdots & s_N \end{bmatrix}^T,$$
$$\mathbf{v}_e(\jmath\varpi\psi_m) = \frac{1}{2\pi} \int_0^{2\pi} e^{\jmath\varpi\cos(\theta-\psi_m)} \mathbf{p}_e(\theta)\, d\theta,$$
$$\mathbf{M}_e = \frac{1}{2\pi} \int_0^{2\pi} \mathbf{p}_e(\theta)\, \mathbf{p}_e^H(\theta)\, d\theta.$$

The minimization of the LSE criterion gives the optimal solution:

$$\mathbf{s}_{2N} = \mathbf{M}_e^{-1} \mathbf{v}_e(\jmath\varpi\psi_m). \tag{24}$$

Let us take a close look at $\mathbf{v}_e(\jmath\varpi\psi_m)$ and $\mathbf{M}_e$. As shown in Appendix A, we have

$$[\mathbf{v}_e(\jmath\varpi\psi_m)]_n = \jmath^n e^{\jmath n\psi_m} J_n(\varpi). \tag{25}$$

The elements of the matrix $\mathbf{M}_e$ are

$$[\mathbf{M}_e]_{ij} = \frac{1}{2\pi} \int_0^{2\pi} e^{\jmath i\theta} e^{-\jmath j\theta}\, d\theta, \tag{26}$$

with $i, j = 0, \pm 1, \ldots, \pm N$. It is easy to verify that

$$\begin{cases} [\mathbf{M}_e]_{ii} = 1, \\ [\mathbf{M}_e]_{ij} = 0, \quad i \neq j \end{cases}.$$

As a result, $\mathbf{M}_e = \mathbf{I}_{2N+1}$, where $\mathbf{I}_{2N+1}$ is the $(2N+1) \times (2N+1)$ identity matrix, and the exponential function given

in (22) can be expressed as

$$\begin{aligned} e^{\jmath\varpi\cos(\theta-\psi_m)} &= \sum_{n=-\infty}^{\infty} \jmath^n J_n(\varpi)\, e^{-\jmath n(\theta-\psi_m)} \\ &= \sum_{n=-\infty}^{\infty} \jmath^n J_n(\varpi)\, e^{\jmath n(\theta-\psi_m)} \\ &= J_0(\varpi) + 2\sum_{n=1}^{\infty} \jmath^n J_n(\varpi)\cos\left[n(\theta-\psi_m)\right], \end{aligned} \tag{27}$$

where $J_n(\varpi)$ is the n th-order Bessel function of the first kind with $J_{-n}(\varpi) = (-1)^n J_n(\varpi)$. Expression (27) is the well-known Jacobi-Anger expansion [40].

Substituting (27) into the beampattern of the fixed beamformer, $\mathbf{h}(\omega)$, we obtain

$$\begin{aligned} \mathcal{B}\left[\mathbf{h}(\omega),\theta\right] &= \sum_{m=1}^{M} H_m^*(\omega)\, e^{\jmath\varpi\cos(\theta-\psi_m)} \\ &= \sum_{m=1}^{M} H_m^*(\omega) \sum_{n=-\infty}^{\infty} \jmath^n J_n(\varpi)\, e^{\jmath n(\theta-\psi_m)} \\ &= \sum_{n=-\infty}^{\infty} e^{\jmath n\theta}\left[\sum_{m=1}^{M} \jmath^n J_n(\varpi)\, e^{-\jmath n\psi_m} H_m^*(\omega)\right]. \end{aligned} \tag{28}$$

If we limit the expansion to the order $\pm N$, $\mathcal{B}\left[\mathbf{h}(\omega),\theta\right]$ can be approximated by

$$\begin{aligned} &\mathcal{B}_{2N}\left[\mathbf{h}(\omega),\theta\right] \\ &= \sum_{n=-N}^{N} e^{\jmath n\theta}\left[\sum_{m=1}^{M} \jmath^n J_n(\varpi)\, e^{-\jmath n\psi_m} H_m^*(\omega)\right], \end{aligned} \tag{29}$$

which is the best approximation of the beampattern from an LSE perspective.

B. Design by Identification

It is assumed that $M \geq 2N+1$. Then, the approximate beampattern in (29) can be rewritten as

$$\mathcal{B}_{2N}\left[\mathbf{h}(\omega),\theta\right] = \sum_{n=-N}^{N} e^{\jmath n\theta} \jmath^n J_n(\varpi)\, \boldsymbol{\psi}_n^T \mathbf{h}^*(\omega), \tag{30}$$

where

$$\boldsymbol{\psi}_n = \begin{bmatrix} e^{-\jmath n\psi_1} & e^{-\jmath n\psi_2} & \cdots & e^{-\jmath n\psi_M} \end{bmatrix}^T. \tag{31}$$

Now, let $\mathcal{B}_{2N}\left[\mathbf{h}(\omega),\theta\right]$ to be same as $\mathcal{B}\left[\mathbf{c}_{2N}(\theta_{\mathrm{s}}),\theta\right]$, we have

$$\begin{aligned} \mathcal{B}_{2N}\left[\mathbf{h}(\omega),\theta\right] &= \mathcal{B}\left[\mathbf{c}_{2N}(\theta_{\mathrm{s}}),\theta\right] \\ &= \mathbf{c}_{2N}^T(\theta_{\mathrm{s}})\,\mathbf{p}_e(\theta) \\ &= \sum_{n=-N}^{N} c_{2N,n}(\theta_{\mathrm{s}})\, e^{\jmath n\theta}. \end{aligned} \tag{32}$$

It follows then that

$$\boldsymbol{\Psi}^*\mathbf{h}^*(\omega) = \mathbf{J}(\varpi)\,\mathbf{c}_{2N}(\theta_{\mathrm{s}}) \tag{33}$$

or, equivalently,

$$\boldsymbol{\Psi}\mathbf{h}(\omega) = \mathbf{J}^*(\varpi)\,\boldsymbol{\Upsilon}^*(\theta_{\mathrm{s}})\,\mathbf{b}_{2N}, \tag{34}$$

where

$$\begin{aligned} \mathbf{J}(\varpi) = \mathrm{diag}\Bigg[&\frac{1}{\jmath^{-N}J_{-N}(\varpi)},\ldots, \\ &\frac{1}{J_0(\varpi)},\ldots,\frac{1}{\jmath^N J_N(\varpi)}\Bigg] \end{aligned} \tag{35}$$

is a $(2N+1)\times(2N+1)$ diagonal matrix and

$$\boldsymbol{\Psi} = \begin{bmatrix} \boldsymbol{\psi}_{-N}^H \\ \vdots \\ \boldsymbol{\psi}_0^H \\ \vdots \\ \boldsymbol{\psi}_N^H \end{bmatrix} \tag{36}$$

is a $(2N+1)\times M$ matrix. Since $\boldsymbol{\Psi}^H$ is a full-column rank matrix, we can take the minimum-norm solution of (34):

$$\mathbf{h}_{\mathrm{MN}}(\omega) = \boldsymbol{\Psi}^H\left(\boldsymbol{\Psi}\boldsymbol{\Psi}^H\right)^{-1}\mathbf{J}^*(\varpi)\,\boldsymbol{\Upsilon}^*(\theta_{\mathrm{s}})\,\mathbf{b}_{2N}. \tag{37}$$

The elements of the matrix $\boldsymbol{\Psi}\boldsymbol{\Psi}^H$ are $\boldsymbol{\psi}_i^H\boldsymbol{\psi}_j$, $i,j = 0,\pm1,\pm2,\ldots,\pm N$. It is clear that

$$\boldsymbol{\psi}_i^H\boldsymbol{\psi}_i = M,$$

while for $i \neq j$,

$$\begin{aligned} \boldsymbol{\psi}_i^H\boldsymbol{\psi}_j &= \sum_{m=1}^{M} e^{\jmath(i-j)\psi_m} \\ &= \sum_{m=1}^{M} e^{\jmath 2\pi(i-j)(m-1)/M} \\ &= \frac{1-e^{\jmath 2\pi(i-j)}}{1-e^{\jmath 2\pi(i-j)/M}} = 0. \end{aligned}$$

As a consequence, $\boldsymbol{\Psi}\boldsymbol{\Psi}^H = M\mathbf{I}_M$, where $\mathbf{I}_M$ is the $M\times M$ identity matrix, and (37) simplifies to

$$\begin{aligned} \mathbf{h}_{\mathrm{MN}}(\omega) &= \frac{1}{M}\boldsymbol{\Psi}^H\mathbf{J}^*(\varpi)\,\boldsymbol{\Upsilon}^*(\theta_{\mathrm{s}})\,\mathbf{b}_{2N} \\ &= \frac{1}{M}\boldsymbol{\Psi}^H\mathbf{J}^*(\varpi)\,\mathbf{c}_{2N}^*(\theta_{\mathrm{s}}). \end{aligned} \tag{38}$$

C. Performance Analysis

Now, let us evaluate the beampattern of $\mathbf{h}_{\mathrm{MN}}(\omega)$ from (28), which it is equal to (7). We have

$$\begin{aligned} \mathcal{B}\left[\mathbf{h}_{\mathrm{MN}}(\omega),\theta\right] &= \sum_{l=-\infty}^{\infty} e^{\jmath l\theta}\jmath^l J_l(\varpi)\,\boldsymbol{\psi}_l^T\mathbf{h}_{\mathrm{MN}}^*(\omega) \\ &= \frac{1}{M}\sum_{l=-\infty}^{\infty} e^{\jmath l\theta}\jmath^l J_l(\varpi)\,\boldsymbol{\psi}_l^T\boldsymbol{\Psi}^T\mathbf{J}(\varpi)\,\mathbf{c}_{2N}(\theta_{\mathrm{s}}). \end{aligned} \tag{39}$$

Using the fact that $\boldsymbol{\psi}_l^T \boldsymbol{\Psi}^T = \mathbf{0}$ for $l \neq mM+n$ with $m \geq 0$ and $n = 0, \pm 1, \pm 2, \ldots, \pm N$, we can express (39) as

$$\begin{aligned}
&\mathcal{B}\left[\mathbf{h}_{\mathrm{MN}}(\omega), \theta\right] \\
&= \sum_{m=0}^{\infty} \jmath^{mM} e^{\jmath mM\theta} \sum_{n=-N}^{N} e^{\jmath n\theta} \frac{J_{mM+n}(\varpi)}{J_n(\varpi)} c_{2N,n}(\theta_{\mathrm{s}}) \\
&= \sum_{n=-N}^{N} e^{\jmath n\theta} c_{2N,n}(\theta_{\mathrm{s}}) + \sum_{n=-N}^{N} \frac{c_{2N,n}(\theta_{\mathrm{s}})}{\jmath^n J_n(\varpi)} \\
&\quad \times \sum_{m=1}^{\infty} \jmath^{mM+n} e^{\jmath(mM+n)\theta} J_{mM+n}(\varpi) \\
&= \mathbf{c}_{2N}^T(\theta_{\mathrm{s}}) \mathbf{p}_e(\theta) + \sum_{n=-N}^{N} \frac{c_{2N,n}(\theta_{\mathrm{s}})}{\jmath^n J_n(\varpi)} \\
&\quad \times \sum_{m=1}^{\infty} e^{\jmath(mM+n)(\theta+\pi/2)} J_{mM+n}(\varpi) \\
&= \mathcal{B}\left[\mathbf{c}_{2N}(\theta_{\mathrm{s}}), \theta\right] + \sum_{n=-N}^{N} \frac{c_{2N,n}(\theta_{\mathrm{s}})}{\jmath^n} \mathcal{S}_n(\varpi, \theta), \qquad (40)
\end{aligned}$$

where

$$\mathcal{S}_n(\varpi, \theta) = \sum_{m=1}^{\infty} e^{\jmath(mM+n)(\theta+\pi/2)} \frac{J_{mM+n}(\varpi)}{J_n(\varpi)} \qquad (41)$$

is a convergent series. Since $mM+n \geq \varpi$ according to (4), $J_{mM+n}(\varpi)/J_n(\varpi)$ is close to 0. The coefficient $c_{2N,n}(\theta_{\mathrm{s}})$ is within the range of $(0,1)$. As a result, the second term on the right-hand side of (40) can be neglected and

$$\mathcal{B}\left[\mathbf{h}_{\mathrm{MN}}(\omega), \theta\right] \approx \mathcal{B}\left[\mathbf{c}_{2N}(\theta_{\mathrm{s}}), \theta\right], \qquad (42)$$

proving that the designed beampattern is very close to the desired directivity pattern. This result is quite interesting; not only $\mathbf{h}_{\mathrm{MN}}(\omega)$ can steer in all directions but its beampattern is almost identical to the desired directivity pattern and is also almost frequency invariant. Since,

$$\mathcal{B}\left[\mathbf{c}_{2N}(\theta_{\mathrm{s}}), \theta_{\mathrm{s}}\right] \approx \mathcal{B}\left[\mathbf{h}_{\mathrm{MN}}(\omega), \theta_{\mathrm{s}}\right] \approx 1, \qquad (43)$$

we deduce that

$$\mathbf{h}_{\mathrm{MN}}^H(\omega) \mathbf{d}(\omega, \theta_{\mathrm{s}}) \approx 1. \qquad (44)$$

The WNG is

$$\begin{aligned}
\mathcal{W}\left[\mathbf{h}_{\mathrm{MN}}(\omega)\right] &= \frac{\left|\mathbf{h}_{\mathrm{MN}}^H(\omega) \mathbf{d}(\omega, \theta_{\mathrm{s}})\right|^2}{\mathbf{h}_{\mathrm{MN}}^H(\omega) \mathbf{h}_{\mathrm{MN}}(\omega)} \\
&= \frac{M \left|\mathbf{h}_{\mathrm{MN}}^H(\omega) \mathbf{d}(\omega, \theta_{\mathrm{s}})\right|^2}{\mathbf{c}_{2N}^T(\theta_{\mathrm{s}}) \mathbf{J}(\varpi) \mathbf{J}^*(\varpi) \mathbf{c}_{2N}^*(\theta_{\mathrm{s}})} \\
&= \frac{M \left|\mathbf{h}_{\mathrm{MN}}^H(\omega) \mathbf{d}(\omega, \theta_{\mathrm{s}})\right|^2}{\mathbf{b}_{2N}^T \mathbf{J}(\varpi) \mathbf{J}^*(\varpi) \mathbf{b}_{2N}} \\
&= \frac{M \left|\mathbf{h}_{\mathrm{MN}}^H(\omega) \mathbf{d}(\omega, \theta_{\mathrm{s}})\right|^2}{\sum_{n=-N}^{N} \frac{b_{2N,n}^2}{J_n^2(\varpi)}} \\
&= \frac{M \left|\mathbf{h}_{\mathrm{MN}}^H(\omega) \mathbf{d}(\omega, \theta_{\mathrm{s}})\right|^2}{\frac{a_{N,0}^2}{J_0^2(\varpi)} + \frac{1}{2} \sum_{n=1}^{N} \frac{a_{N,n}^2}{J_n^2(\varpi)}} \\
&\approx \frac{M}{\frac{a_{N,0}^2}{J_0^2(\varpi)} + \frac{1}{2} \sum_{n=1}^{N} \frac{a_{N,n}^2}{J_n^2(\varpi)}}. \qquad (45)
\end{aligned}$$

We observe that the WNG depends clearly on M but M is not connected to N (note, however, that the design of a directivity pattern of order N requires at least $M = 2N+1$ microphones). As a consequence, for a fixed value of the order, we can always improve the WNG by increasing the number of sensors.

In the same way, the DF is

$$\begin{aligned}
\mathcal{D}\left[\mathbf{h}_{\mathrm{MN}}(\omega)\right] &= \frac{\left|\mathbf{h}_{\mathrm{MN}}^H(\omega) \mathbf{d}(\omega, \theta_{\mathrm{s}})\right|^2}{\mathbf{h}_{\mathrm{MN}}^H(\omega) \boldsymbol{\Gamma}_{\mathrm{d}}(\omega) \mathbf{h}_{\mathrm{MN}}(\omega)} \\
&= \frac{M^2 \left|\mathbf{h}_{\mathrm{MN}}^H(\omega) \mathbf{d}(\omega, \theta_{\mathrm{s}})\right|^2}{\mathbf{c}_{2N}^T(\theta_{\mathrm{s}}) \mathbf{J}(\varpi) \boldsymbol{\Psi} \boldsymbol{\Gamma}_{\mathrm{d}}(\omega) \boldsymbol{\Psi}^H \mathbf{J}^*(\varpi) \mathbf{c}_{2N}^*(\theta_{\mathrm{s}})}. \qquad (46)
\end{aligned}$$

Since $\boldsymbol{\Gamma}_{\mathrm{d}}(\omega)$ is a circulant matrix, it can be decomposed as [41]

$$\boldsymbol{\Gamma}_{\mathrm{d}}(\omega) = \mathbf{F} \boldsymbol{\Lambda}(\omega) \mathbf{F}^H, \qquad (47)$$

where

$$\mathbf{F} = \frac{1}{\sqrt{M}} \begin{bmatrix} \mathbf{f}_1 & \mathbf{f}_2 & \cdots & \mathbf{f}_M \end{bmatrix} \qquad (48)$$

is the Fourier matrix and

$$\boldsymbol{\Lambda}(\omega) = \mathrm{diag}\left[\lambda_1(\omega), \lambda_2(\omega), \ldots, \lambda_M(\omega)\right] \qquad (49)$$

is a diagonal matrix. The eigenvectors in (48) can be written in terms of the positions of the sensors, i.e.,

$$\begin{aligned}
\mathbf{f}_m &= \begin{bmatrix} 1 & e^{\jmath 2\pi(m-1)/M} & \cdots & e^{\jmath 2\pi(m-1)(M-1)/M} \end{bmatrix}^T \\
&= \begin{bmatrix} e^{\jmath(m-1)\psi_1} & e^{\jmath(m-1)\psi_2} & \cdots & e^{\jmath(m-1)\psi_M} \end{bmatrix}^T \\
&= \boldsymbol{\psi}_{m-1}^*. \qquad (50)
\end{aligned}$$

Therefore, the Fourier matrix is also

$$\mathbf{F} = \frac{1}{\sqrt{M}} \left[\boldsymbol{\psi}_0^* \quad \boldsymbol{\psi}_1^* \quad \cdots \quad \boldsymbol{\psi}_{M-1}^* \right] = \frac{1}{\sqrt{M}} \left[\boldsymbol{\Psi}_1 \quad \boldsymbol{\Psi}_2 \quad \boldsymbol{\Psi}_3 \right], \tag{51}$$

where

$$\boldsymbol{\Psi}_1 = \left[\boldsymbol{\psi}_0^* \quad \boldsymbol{\psi}_1^* \quad \cdots \quad \boldsymbol{\psi}_N^* \right],$$
$$\boldsymbol{\Psi}_2 = \left[\boldsymbol{\psi}_{N+1}^* \quad \boldsymbol{\psi}_{N+2}^* \quad \cdots \quad \boldsymbol{\psi}_{M-N-1}^* \right],$$
$$\boldsymbol{\Psi}_3 = \left[\boldsymbol{\psi}_{M-N}^* \quad \boldsymbol{\psi}_{M-N+1}^* \quad \cdots \quad \boldsymbol{\psi}_{M-1}^* \right].$$

The other matrix of interest $\boldsymbol{\Psi}^H$ can be rewritten as

$$\boldsymbol{\Psi}^H = \left[\boldsymbol{\psi}_N^* \quad \cdots \quad \boldsymbol{\psi}_0^* \quad \cdots \quad \boldsymbol{\psi}_N \right]. \tag{52}$$

Hence,

$$\mathbf{F}^H \boldsymbol{\Psi}^H = \frac{1}{\sqrt{M}} \begin{bmatrix} \boldsymbol{\Psi}_1^H \\ \boldsymbol{\Psi}_2^H \\ \boldsymbol{\Psi}_3^H \end{bmatrix} \boldsymbol{\Psi}^H = \sqrt{M} \begin{bmatrix} \mathbf{I}_{N+1} & \mathbf{0} \\ \mathbf{0} & \mathbf{0} \\ \mathbf{0} & \mathbf{I}_N \end{bmatrix}, \tag{53}$$

where $\mathbf{I}_{N+1}$ and $\mathbf{I}_N$ are the antidiagonal identity matrices of sizes $(N+1) \times (N+1)$ and $N \times N$, respectively, and

$$\begin{aligned} \boldsymbol{\Psi} \boldsymbol{\Gamma}_{\mathrm{d}} (\omega) \boldsymbol{\Psi}^H &= \boldsymbol{\Psi} \mathbf{F} \boldsymbol{\Lambda} (\omega) \mathbf{F}^H \boldsymbol{\Psi}^H \\ &= M \mathrm{diag} \left[\lambda_{N+1}(\omega), \lambda_N(\omega), \ldots, \lambda_1(\omega), \right. \\ &\quad \left. \lambda_M(\omega), \ldots, \lambda_{M-N+1}(\omega) \right] \\ &= \boldsymbol{\Lambda}_{2N} (\omega), \end{aligned} \tag{54}$$

where $\boldsymbol{\Lambda}_{2N}(\omega)$ is a diagonal matrix of size $(2N+1) \times (2N+1)$. Taking into account the symmetry of the eigenvalues of a circulant matrix, i.e., $\lambda_{m+1}(\omega) = \lambda_{M-N+1}(\omega)$, we can express (54) as

$$\begin{aligned} \boldsymbol{\Lambda}_{2N} (\omega) &= M \mathrm{diag} \left[\lambda_{N+1}(\omega), \lambda_N(\omega), \ldots, \lambda_1(\omega), \right. \\ &\quad \left. \lambda_2(\omega), \ldots, \lambda_{N+1}(\omega) \right]. \end{aligned} \tag{55}$$

Substituting the previous expression into (46), we can finally write the DF as

$$\begin{aligned} \mathcal{D} \left[\mathbf{h}_{\mathrm{MN}} (\omega) \right] &= \frac{M \left| \mathbf{h}_{\mathrm{MN}}^H (\omega) \mathbf{d} (\omega, \theta_{\mathrm{s}}) \right|^2}{\dfrac{\lambda_1(\omega) a_{N,0}^2}{J_0^2(\varpi)} + \dfrac{1}{2} \displaystyle\sum_{n=1}^{N} \dfrac{\lambda_{n+1}(\omega) a_{N,n}^2}{J_n^2(\varpi)}} \\ &\approx \frac{M}{\dfrac{\lambda_1(\omega) a_{N,0}^2}{J_0^2(\varpi)} + \dfrac{1}{2} \displaystyle\sum_{n=1}^{N} \dfrac{\lambda_{n+1}(\omega) a_{N,n}^2}{J_n^2(\varpi)}}. \end{aligned} \tag{56}$$

Generally, the ratio $\lambda_{n+1}(\omega)/J_n^2(\varpi)$ in (56) does not change much with frequency. So, the DF is almost frequency invariant. However, this ratio may change significantly when the Bessel function, $J_n(\varpi)$, approaches to zero. In this case, the beamformer may suffer from significant degradation in performance, which will be discussed in the next subsection.

D. Impact of Bessel Nulls

It is seen from (33)–(35) as well as from Appendix A that the beamforming coefficients are functions of the Bessel functions of different orders. The beamformer may suffer from significant degradation at some frequencies where those Bessel functions approach zero. One way to circumvent this problem is through using a rigid baffled circular array, where the sensors are mounted on a rigid, infinite cylinder (or sphere), and the sound wave is scattered by the cylinder [18], [44]. Then, the pressure is the superposition of the incident pressure and scattered pressure. In this case, the Bessel function $J_n(\varpi)$ in (27) is replaced by [18], [44]

$$\bar{J}_n(\varpi) = J_n(\varpi) - \frac{J_n'(\epsilon\varpi)}{H_n'^{(1)}(\epsilon\varpi)} H_n^{(1)}(\varpi), \tag{57}$$

where $H_n^{(1)}(\varpi)$ is the n th-order Hankel function of the first kind, the superscript $'$ denotes the derivative operation, and $\epsilon = r_a/r$, with r_a being the radius of the cylinder.

Another way to deal with the Bessel null problem is through using a concentric circular array, which consists of multiple rings of microphones. With this approach, the beamformer design process is similar to that of circular arrays; but the performance of the resulting beamformer is significantly less affected or even unaffected by Bessel nulls [45].

V. Evaluation and Analysis

In this section, we study the performance of the developed beamforming approach in (38) through simulations. The proposed frequency-invariant beamformer is deduced from the optimal approximation of the beampattern from an LSE perspective, so we call it FIB-LSE for short. In the remainder of this paper, unless specified otherwise, we only focus on the design of the second-order supercardioid [10], whose coefficients are given by

$$\mathbf{b}_{2N} = \left[0.1035 \quad 0.242 \quad 0.309 \quad 0.242 \quad 0.1035 \right]^T.$$

A. Performance Evaluation

We first study the steering ability of the FIB-LSE. We set $M = 8$, $r = 1.5$ cm, $f = 1000$ Hz, and $\theta_{\mathrm{s}} \in \{0^\circ, 15^\circ, 30^\circ, 60^\circ, 80^\circ, 100^\circ, 120^\circ, 150^\circ\}$. The designed beampatterns are plotted in Fig. 1, where red arrows point to the desired directions. Fig. 1(a) plots the beampattern of the FIB-LSE steered in the direction $\theta_{\mathrm{s}} = 0^\circ$, which has a one at 0° and two nulls at 106° and 153°. Fig. 1(b)–(h) show beampatterns of the FIB-LSE steered to other directions. One can see that perfect steering is possible to these directions and all beampatterns are symmetric about the axis $\theta_{\mathrm{s}} \leftrightarrow \theta_{\mathrm{s}} + \pi$.

We then evaluate the WNG and DF performance of the FIB-LSE. Fig. 2 plots the DF and the WNG as a function of frequency with $r = 1.5$ cm, for $M \in \{5, 8, 12\}$ (note that increasing the number of microphones with fixed radius leads to a smaller interelement spacing). As one can see, the beamformer has a very small value of WNG at low frequencies, indicating that this beamformer significantly amplifies white noise. It is seen

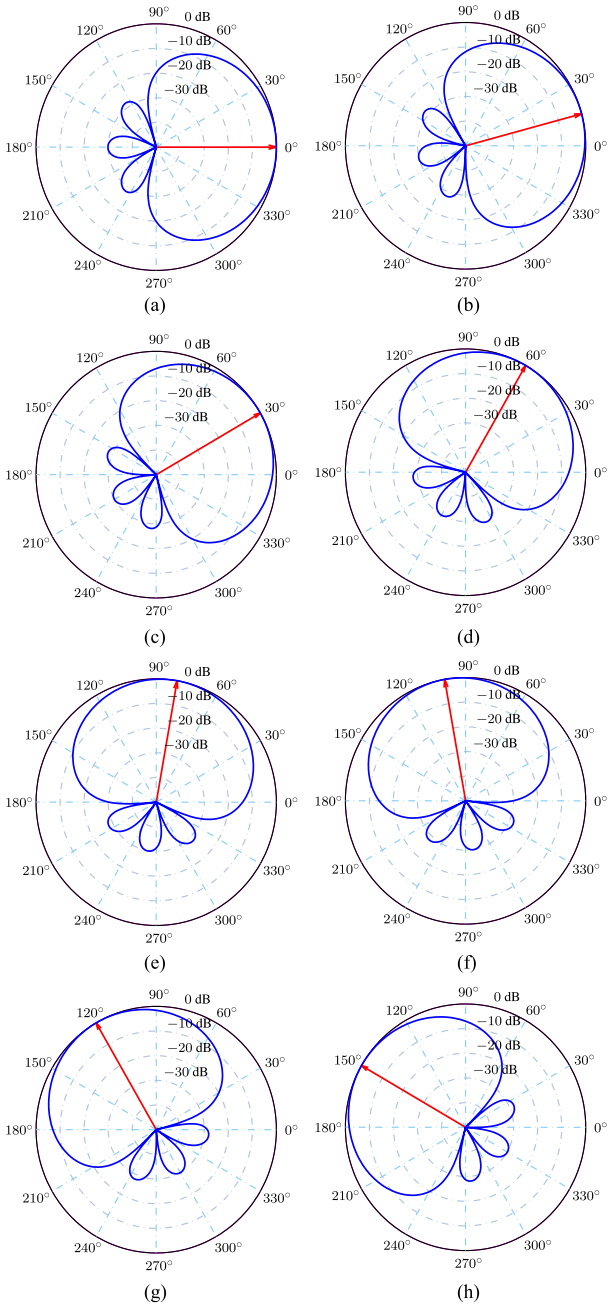

Fig. 1. Beampatterns of the FIB-LSE for different steering directions, θ_s: (a) $\theta_s = 0°$, (b) $\theta_s = 15°$, (c) $\theta_s = 30°$, (d) $\theta_s = 60°$, (e) $\theta_s = 80°$, (f) $\theta_s = 100°$, (g) $\theta_s = 120°$, and (h) $\theta_s = 150°$. Conditions of simulation: $M = 8$, $r = 1.5$ cm, and $f = 1000$ Hz.

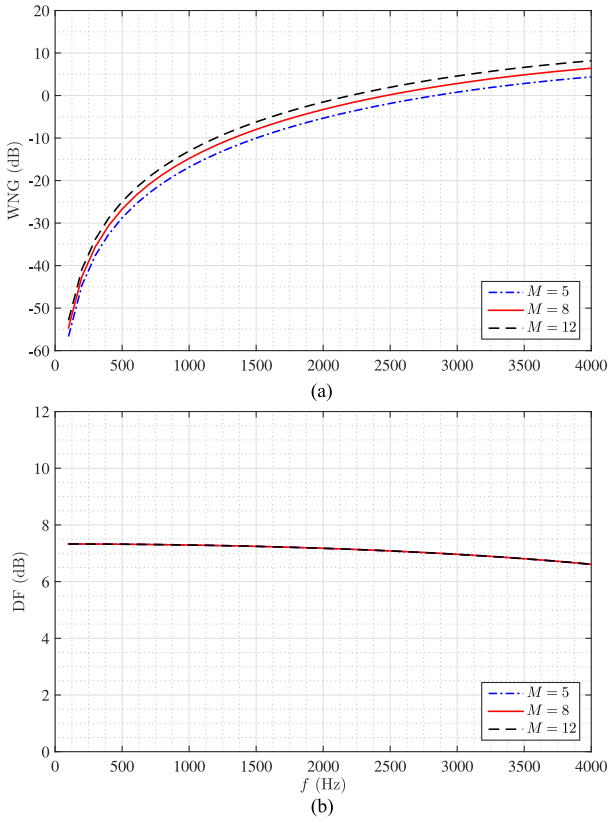

Fig. 2. DF and WNG of the FIB-LSE as a function of the frequency, f, for different numbers of microphones: (a) DF and (b) WNG. Conditions of simulation: $r = 1.5$ cm.

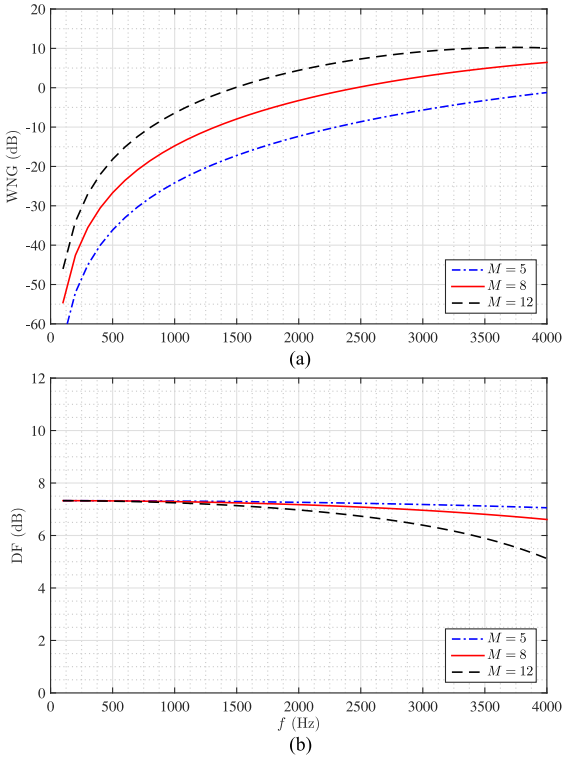

Fig. 3. DF and WNG of the FIB-LSE as a function of the frequency, f, for different numbers of microphones: (a) DF and (b) WNG. Conditions of simulation: $\delta = 1.15$ cm.

that for fixed values of the order and the radius, increasing the number of microphones can slightly improve the WNG without changing the DF. Certainly, increasing both the number of microphones, i.e., the value of M and the interelement spacing, δ, can further improve the WNG. Fig. 3 plots the WNG and the DF as a function of frequency with $\delta = 1.15$ cm [r is obtained according to (3)], for $M \in \{5, 8, 12\}$. By comparing with Fig. 2, it is clearly seen that the WNG is considerably improved when increasing the number of microphones. However, this comes at

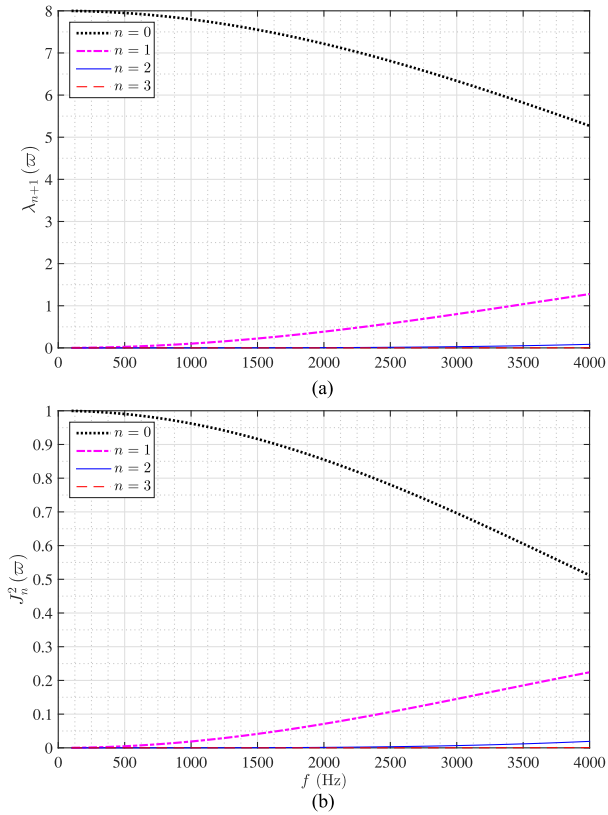

Fig. 4. The value of $\lambda_{n+1}(\varpi)$ and $J_n^2(\varpi)$ as a function of the frequency, f, for different orders, n: (a) $\lambda_{n+1}(\varpi)$ and (b) $J_n^2(\varpi)$. Conditions of simulation: $M = 8$ and $r = 1.5$ cm.

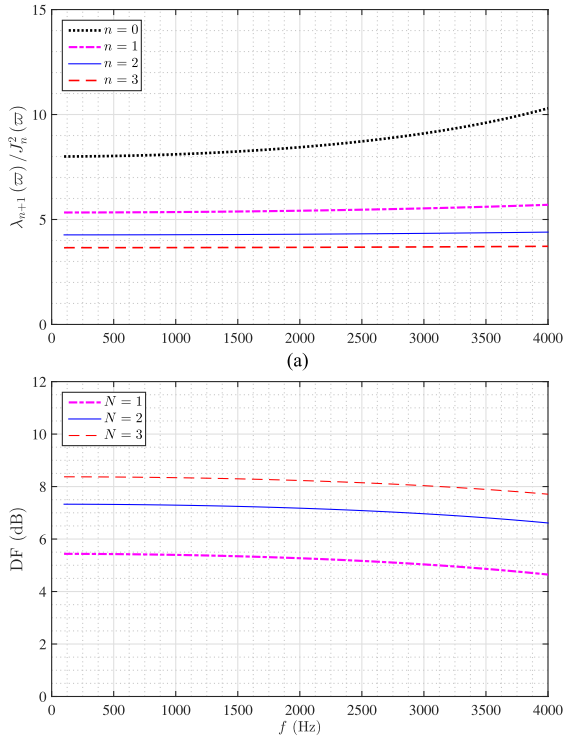

Fig. 5. The value of $\lambda_{n+1}(\varpi)/J_n^2(\varpi)$ and the DF as a function of the frequency, f, for different orders, n (or N): (a) $\lambda_{n+1}(\varpi)/J_n^2(\varpi)$ and (b) DF. Conditions of simulation: $M = 8$ and $r = 1.5$ cm.

a price of a larger array aperture and the DF degradation at high frequencies.

While the beampattern is almost frequency invariant, it is worth noticing that the DF suffers from slight degradation at high frequencies as seen in Fig. 3. As shown in (56), to achieve a frequency-invariant beampattern, $\lambda_{n+1}(\omega)/J_n^2(\varpi)$ should be a constant. To see this clearly, we set $M = 8$, $r = 1.5$ cm, and show the eigenvalue, $\lambda_{n+1}(\omega)$, the squared Bessel function, $J_n^2(\varpi)$, the ratio between $\lambda_{n+1}(\varpi)$ and $J_n^2(\varpi)$, and the DF as a function of frequency. The results are plotted in Figs. 4 and 5. Fig. 4 shows that the eigenvalues and the squared Bessel functions have almost the same trend with frequency. Fig. 5(a) shows that the ratio between $\lambda_{n+1}(\varpi)$ and $J_n^2(\varpi)$ remains broadly constant over frequency for all orders except for $n = 0$. For $n = 0$, the ratio first keeps constant and then increases with frequency, which explains the reason for the DF degradation at high frequencies. [In fact, this is mainly caused by the zeros of the Bessel function, the value of $\lambda_{n+1}(\omega)/J_n^2(\varpi)$ changes near the zeros. Since the lower-order Bessel function's first zero appears at a lower frequency, the performance degradation of a small size array is mainly caused by the low-order components.] As shown in Fig. 5(b), the DF with different orders, N, suffers from similar performance degradation at high frequencies. Note that this problem can be circumvented through using concentric circular microphone arrays, which is, however, beyond the scope of this paper.

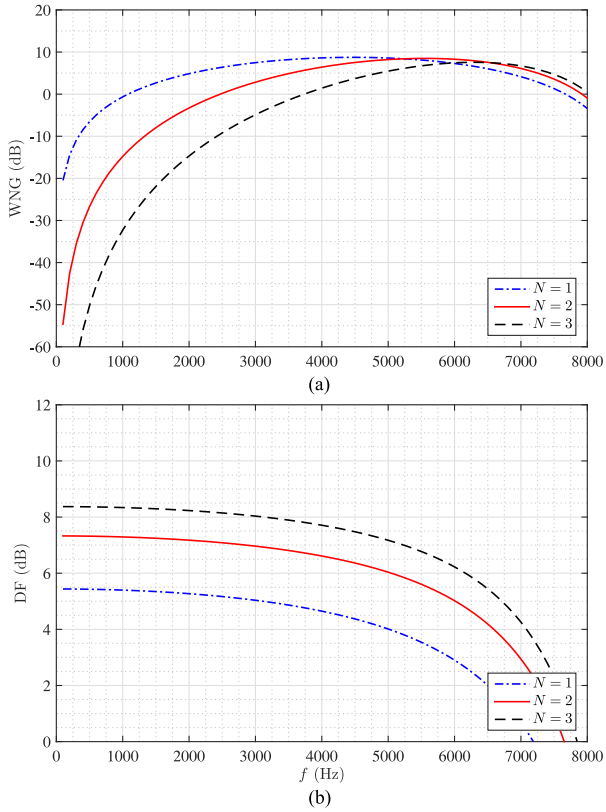

Fig. 6. DF and WNG of the FIB-LSE a function of the frequency, f, for different orders, N: (a) DF and (b) WNG. Conditions of simulation: $M = 8$ and $r = 1.5$ cm.

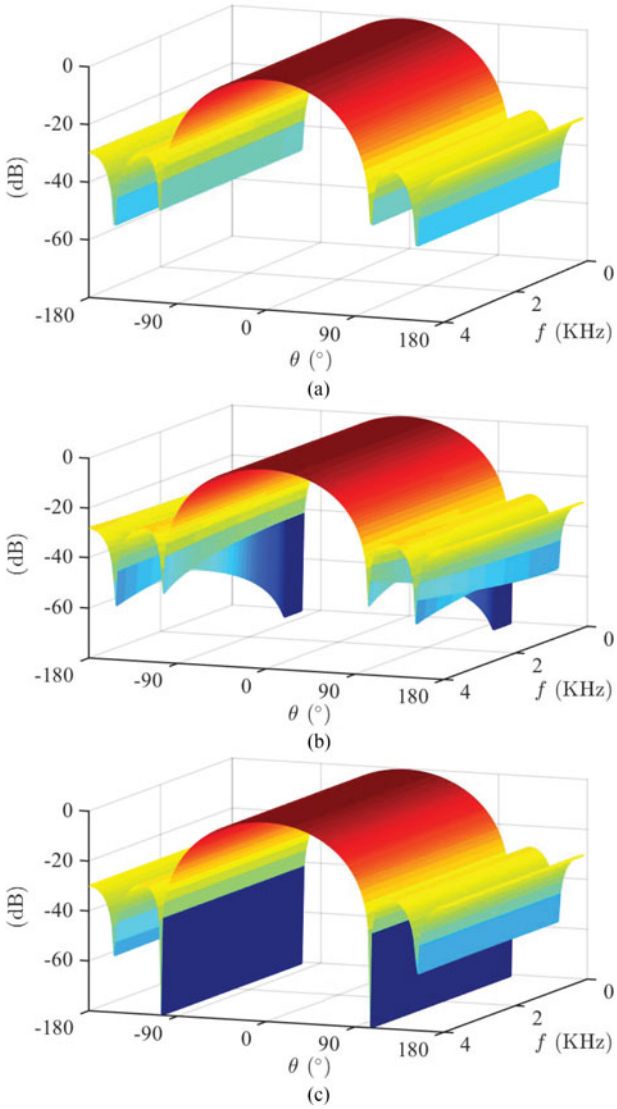

Fig. 7. Three-dimensional beampatterns of the CDMA and the FIB-LSE: (a) CDMA design with null constraints, (b) CDMA design with Jacob-Anger expansion, and (c) FIB-LSE. Conditions of simulation: $M = 8$, $r = 1.5$ cm, and $\theta_s = 0$.

In this simulation, we investigate how the FIB-LSE beamformer behaves at high frequencies with spatial aliasing. Fig. 6 plots the DF and the WNG of the FIB-LSE beamformer, both as a function of the frequency with $M = 8$, $r = 1.5$ cm, for $N \in \{1, 2, 3\}$, where the coefficients of the first-order and third-order supercardioids are, respectively,

$$\mathbf{b}_{2N} = \begin{bmatrix} 0.293 & 0.414 & 0.293 \end{bmatrix}^T$$

and

$$\mathbf{b}_{2N} = \begin{bmatrix} 0.036 & 0.1185 & 0.216 & 0.259 & 0.216 & 0.1185 & 0.036 \end{bmatrix}^T.$$

Clearly, both the DF and the WNG suffer from serious performance degradation when spatial aliasing occurs, especially at frequencies higher than 6 KHz. There are different ways to deal with aliasing problem, most of which require physical changes to the microphone array [43], [45]. However, this is again beyond the main thrust of the paper.

B. Performance Comparison

In this subsection, we compare the proposed FIB-LSE with CDMA and CHB.

1) Comparison With CDMA: We first compare the proposed FIB-LSE with CDMA [30], where the CDMA filters are obtained by solving a linear system of equations determined by the null constraints from the desired directivity pattern or by approximating the beamformer beampattern with the Jacobi-Anger expansion. The proposed FIB-LSE is basically a generalization and an improvement of the CDMA developed in [30], with many advantages as described bellow.

1) The CDMA filters designed with the null constraints or the Jacobi-Anger expansion is guarantied to steer only to the M different angles ψ_m, $m = 1, 2, \ldots, M$, but the developed FIB-LSE can steer to any look direction in the plane where the sensors are located.
2) FIB-LSE is simpler to design since no extra symmetry constraints are needed as in [30], and it is numerically more robust and reduces the computational complexity since only multiplications are needed (the CDMA in [30] needs matrix inversions).
3) FIB-LSE exhibits a better frequency-invariant property since its beampatterns are by theory almost frequency invariant.

We compare the three-dimensional beampatterns of the FIB-LSE and CDMA designed with the null constraints and the Jacob-Anger expansion. Fig. 7 shows that all the beamformers can form beampatterns, which are almost frequency invariant, but the FIB-LSE has deeper nulls and exhibits a better frequency-invariant property.

2) Comparison With CHB: It is also worthy to compare the FIB-LSE with the CHB [17]–[19]. As shown in Appendix B, the CHB can be considered as a special case of the FIB-LSE, i.e., the CHB designs the hypercardioid pattern. This is an important property, which gives new insights into the design of frequency-invariant beampatterns. It also establishes the theoretical relationship between CDMA and CHB, which makes it possible to design CDMA and CHB under the same framework.

Let us consider the design, with the FIB-LSE, of the second-order dipole, cardioid, supercardioid, and hypercardioid (for this one, the FIB-LSE and CHB are the same), and compare their beampatterns, WNGs, and DFs. The coefficients of the second-order dipole, cardioid, and hypercardioid are given by

$$\text{dipole}: \mathbf{b}_{2N} = \begin{bmatrix} 0.25 & 0 & 0.5 & 0 & 0.25 \end{bmatrix}^T,$$

$$\text{cardioid}: \mathbf{b}_{2N} = \begin{bmatrix} 0.125 & 0.25 & 0.25 & 0.25 & 0.125 \end{bmatrix}^T,$$

$$\text{hypercardioid}: \mathbf{b}_{2N} = \begin{bmatrix} 0.2 & 0.2 & 0.2 & 0.2 & 0.2 \end{bmatrix}^T.$$

Fig. 8 plots the three-dimensional beampatterns. The corresponding WNGs and DFs as a function of frequency are plotted in Fig. 9. For reference, the beampattern, WNG and DF of the DS beamformer are also shown, respectively, in Figs. 8 and 9. As seen, except for the DS beamformer, all the other beamformers can form frequency-invariant beampatterns. While the DS beamformer has a large WNG, its directivity is very limited.

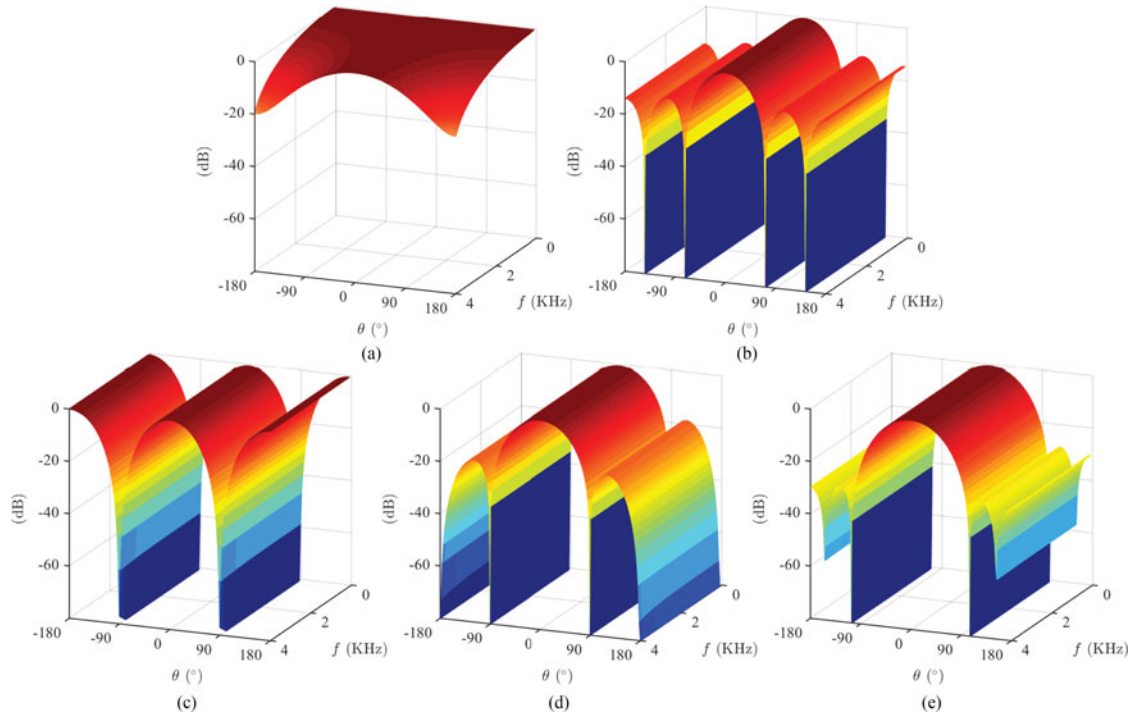

Fig. 8. Three-dimensional beampatterns of the DS, CHB, and FIB-LSE: (a) DS, (b) CHB, (c) FIB-LSE: dipole, (d) FIB-LSE: cardioid, and (e) FIB-LSE: supercardioid. Conditions of simulation: $M = 8$, $r = 1.5$ cm, and $\theta_s = 0$.

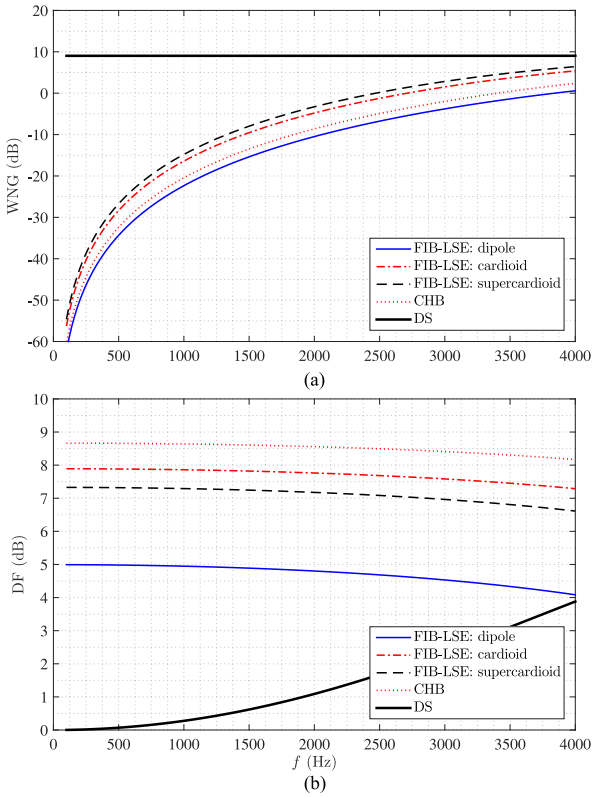

Fig. 9. DFs and WNGs of the DS, CHB, and FIB-LSE as a function of the frequency, f: (a) DF and (b) WNG. Conditions of simulation: $M = 8$, $r = 1.5$ cm, and $\theta_s = 0$.

Note that the optimal choice of the directivity pattern should depend on practical situations.

VI. Conclusion

Frequency-invariant beamforming has been extensively studied in the literature as it has the great potential to be used in processing broadband signals. This paper studied the design of frequency-invariant beampatterns with UCAs. We first expressed the desired symmetric directivity pattern as a function of circular harmonics and introduce the important steering information into it. An optimal approximation of the beamformer beampattern in an LSE sense was subsequently presented and the frequency-invariant beamformer was derived with this approximation. The developed approach can be used to design any desired symmetric directivity pattern, in which the deduced beampattern is almost frequency invariant and its main beam can be pointed at any wanted direction in the plane where the sensors are located. Moreover, the proposed approach can be viewed as a generalization and improvement of CDMA. It is also shown that the beampattern designed by the well known CHB method is a particular case of the beampatterns designed by the developed method.

Appendix A
Derivation of (25)

The vector $\mathbf{v}_e\left(\jmath\varpi\psi_m\right)$ consists of $2N+1$ elements, which are written as

$$\left[\mathbf{v}_e\left(\jmath\varpi\psi_m\right)\right]_n = \frac{1}{2\pi}\int_0^{2\pi} e^{\jmath\varpi\cos(\theta-\psi_m)}e^{\jmath n\theta}d\theta$$
$$= \frac{\jmath^n e^{\jmath n\psi_m}}{2\pi}\xi, \tag{58}$$

where $n = 0, \pm 1, \ldots, \pm N$, and

$$\xi = \int_0^{2\pi} e^{\jmath \varpi \cos(\psi_m - \theta)} e^{-\jmath n(\psi_m - \theta + \pi/2)} d\theta,$$

For ease of notation, let us set $t = \psi_m - \theta + \pi/2$. It follows then

$$\begin{aligned}\xi &= -\int_{\psi_m + \pi/2}^{\psi_m - 3\pi/2} e^{\jmath \varpi \cos(t - \pi/2)} e^{-\jmath n t} dt \\ &= \int_{\psi_m - 3\pi/2}^{\psi_m + \pi/2} e^{\jmath(\varpi \sin t - nt)} dt \\ &= \int_{\psi_m - 3\pi/2}^{0} e^{\jmath(\varpi \sin t - nt)} dt \\ &\quad + \int_0^{2\pi} e^{\jmath(\varpi \sin t - nt)} dt \\ &\quad + \int_{2\pi}^{\psi_m + \pi/2} e^{\jmath(\varpi \sin t - nt)} dt. \end{aligned} \tag{59}$$

With some simple mathematical manipulation, we obtain

$$\xi = \int_0^{2\pi} e^{\jmath(\varpi \sin t - nt)} dt = 2\pi J_n(\varpi). \tag{60}$$

Substituting (60) into (58) gives (25).

Appendix B
Relation Between the FIB-LSE and the CHB

In this appendix, we show that the CHB is a particular case of the FIB-LSE.

Substituting the definitions of $\mathbf{\Psi}$, $\mathbf{J}(\varpi)$, and $\mathbf{c}_{2N}(\theta_s)$ into (38), it is easy to deduce the mth ($m = 1, 2, \ldots, M$) coefficient of the FIB-LSE filter:

$$H_m(\omega) = \frac{1}{M} \sum_{n=-N}^{N} \frac{b_{2N,n}}{[\jmath^n J_n(\varpi)]^*} e^{\jmath n \psi_m} e^{\jmath n \theta_s}. \tag{61}$$

We then derive the coefficients of the CHB filter, where the design process is based on the one given in [17]. The CHB first represents the measured sound pressure with a circular Fourier series as

$$C_n(\omega) = \frac{1}{M} \sum_{m=1}^{M} Y_m(\omega) e^{-\jmath n \psi_m}, \tag{62}$$

where $n = 0, \pm 1, \ldots, \pm N$, N is the order of the CHB, and $Y_m(\omega)$ is the mth microphone signal. Then, the array output of the CHB is

$$Z(\omega) = \frac{1}{2N+1} \sum_{n=-N}^{N} \frac{1}{\jmath^n J_n(\varpi)} e^{-\jmath n \theta_s} C_n(\omega). \tag{63}$$

Substituting (62) into (63), we get

$$\begin{aligned} Z(\omega) &= \sum_{m=1}^{M} Y_m(\omega) \frac{1}{M(2N+1)} \\ &\quad \times \sum_{n=-N}^{N} \frac{1}{\jmath^n J_n(\varpi)} e^{-\jmath n \psi_m} e^{-\jmath n \theta_s}. \end{aligned} \tag{64}$$

From the previous expression, we easily see that the mth coefficient of the CHB filter can be written as

$$H_m(\omega) = \frac{1}{M(2N+1)} \sum_{n=-N}^{N} \frac{1}{[\jmath^n J_n(\varpi)]^*} e^{\jmath n \psi_m} e^{\jmath n \theta_s}. \tag{65}$$

Comparing (61) with (65), it is clearly seen that the CHB is a special case of the FIB-LSE, i.e.,

$$\mathbf{b}_{2N} = \frac{1}{2N+1} \begin{bmatrix} 1 & \cdots & 1 & \cdots & 1 \end{bmatrix}^T,$$

which corresponds to a hypercardioid pattern in the FIB-LSE [30].

References

[1] H. Cox, R. Zeskind, and M. Owen, "Robust adaptive beamforming," *IEEE Trans. Acoust., Speech, Signal Process.*, vol. ASSP-35, no. 10, pp. 1365–1376, Oct. 1987.

[2] G. W. Elko and J. Meyer, "Microphone arrays," in *Springer Handbook of Speech Processing*, J. Benesty, M. M. Sondhi, and Y. Huang, Eds.. Berlin, Germany: Springer-Verlag, 2008, ch. 48, pp. 1021–1041.

[3] C. Li, J. Benesty, G. Huang, and J. Chen, "Subspace superdirective beamformers based on joint diagonalization," in *Proc. IEEE Int. Conf. Acoust., Speech Signal Process.*, 2016, pp. 400–404.

[4] N. Ito, H. Shimizu, N. Ono, and S. Sagayama, "Diffuse noise suppression using crystal-shaped microphone arrays," *IEEE Trans. Audio, Speech, Lang. Process.*, vol. 19, no. 7, pp. 2101–2110, Sep. 2011.

[5] Y. Wang, Y. Yang, Y. Ma, and Z. He, "Robust high-order superdirectivity of circular sensor arrays," *J. Acoust. Soc. Amer.*, vol. 136, no. 4, pp. 1712–1724, 2014.

[6] S. Koyama, K. Furuya, Y. Hiwasaki, Y. Haneda, and Y. Suzuki, "Wave field reconstruction filtering in cylindrical harmonic domain for with-height recording and reproduction," *IEEE/ACM Trans. Audio, Speech, Lang. Process.*, vol. 22, no. 10, pp. 1546–1557, Oct. 2014.

[7] Y. Zeng and R. C. Hendriks, "Distributed delay and sum beamformer for speech enhancement via randomized gossip," *IEEE/ACM Trans. Audio, Speech, Lang. Process.*, vol. 22, no. 1, pp. 260–273, Jan. 2014.

[8] R. Berkun, I. Cohen, and J. Benesty, "Combined beamformers for robust broadband regularized superdirective beamforming," *IEEE/ACM Trans. Audio, Speech, Lang. Process.*, vol. 23, no. 5, pp. 877–886, May 2015.

[9] G. Huang, J. Benesty, and J. Chen, "Superdirective beamforming based on the Krylov matrix," *IEEE/ACM Trans. Audio, Speech, Lang. Process.*, vol. 24, no. 12, pp. 2531–2543, Dec. 2016.

[10] J. Benesty and J. Chen, *Study and Design of Differential Microphone Arrays*. Berlin, Germany: Springer-Verlag, 2012.

[11] J. Flanagan, J. Johnston, R. Zahn, and G. Elko, "Computer-steered microphone arrays for sound transduction in large rooms," *J. Acoust. Soc. Amer.*, vol. 78, pp. 1508–1518, Jul. 1985.

[12] J. Capon, "High-resolution frequency-wavenumber spectrum analysis," *Proc. IEEE*, vol. 57, no. 8, pp. 1408–1418, Aug. 1969.

[13] G. W. Elko, "Differential microphone arrays," in *Audio Signal Processing for Next-Generation Multimedia Communication Systems*. Berlin, Germany: Springer, 2004, pp. 11–65.

[14] E. D. Sena, H. Hacihabiboglu, and Z. Cvetkovic, "On the design and implementation of higher-order differential microphones," *IEEE Trans. Audio, Speech, Lang. Process.*, vol. 20, no. 1, pp. 162–174, Jan. 2012.

[15] T. D. Abhayapala and A. Gupta, "Higher order differential-integral microphone arrays," *J. Acoust. Soc. Amer.*, vol. 136, pp. 227–233, May 2010.

[16] L. Zhao, J. Benesty, and J. Chen, "Design of robust differential microphone arrays," *IEEE/ACM Trans. Audio, Speech, Lang. Process.*, vol. 22, pp. 1455–1466, Oct. 2014.

[17] E. Tiana-Roig, F. Jacobsen, and E. Fernandez-Grande , "Beamforming with a circular microphone array for localization of environmental noise sources," *J. Acoust. Soc. Amer.*, vol. 128, no. 6, pp. 3535–3542, 2010.
[18] E. Tiana-Roig, F. Jacobsen, and E. Fernandez-Grande , "Beamforming with a circular array of microphones mounted on a rigid sphere (L)," *J. Acoust. Soc. Amer.*, vol. 130, no. 3, pp. 1095–1098, 2011.
[19] A. M. Torres, M. Cobos, B. Pueo, and J. J. Lopez, "Robust acoustic source localization based on modal beamforming and time–frequency processing using circular microphone arrays," *J. Acoust. Soc. Amer.*, vol. 132, no. 3, pp. 1511–1520, 2012.
[20] B. Rafaely and D. Khaykin, "Optimal model-based beamforming and independent steering for spherical loudspeaker arrays," *IEEE Trans. Audio, Speech, Lang. Process.*, vol. 19, no. 7, pp. 2234–2238, Sep. 2011.
[21] H. Teutsch and W. Kellermann, "Acoustic source detection and localization based on wavefield decomposition using circular microphone arrays," *J. Acoust. Soc. Amer.*, vol. 120, pp. 2724–2736, Nov. 2006.
[22] B. Rafaely, "Analysis and design of spherical microphone arrays," *IEEE Trans. Speech Audio Process.*, vol. 13, no. 1, pp. 135–142, Jan. 2005.
[23] M. Park and B. Rafaely, "Sound-field analysis by plane-wave decomposition using spherical microphone array," *J. Acoust. Soc. Amer.*, vol. 118, pp. 3094–3103, Nov. 2005.
[24] H. Teutsch, *Modal Array Signal Processing: Principles and Applications of Acoustic Wavefield Decomposition*. Berlin, Germany: Springer, 2007.
[25] S. Yan, H. Sun, U. P. Svensson, X. Ma, and J. M. Hovem, "Optimal modal beamforming for spherical microphone arrays," *IEEE Trans. Audio, Speech, Lang. Process.*, vol. 19, no. 2, pp. 361–371, Feb. 2011.
[26] H. Sun, W. Kellermann, E. Mabande, and K. Kowalczyk, "Localization of distinct reflections in rooms using spherical microphone array eigenbeam processing," *J. Acoust. Soc. Amer.*, vol. 131, pp. 2828–2840, Apr. 2012.
[27] S. Koyama, K. Furuya, K. Wakayama, S. Shimauchi, and H. Saruwatari, "Analytical approach to transforming filter design for sound field recording and reproduction using circular arrays with a spherical baffle," *J. Acoust. Soc. Amer.*, vol. 139, no. 3, pp. 1024–1036, 2016.
[28] C. Bouchard, D. I. Havelock, and M. Bouchard, "Beamforming with microphone arrays for directional sources," *J. Acoust. Soc. Amer.*, vol. 125, no. 4, pp. 2098–2104, 2009.
[29] G. W. Elko, "Microphone array systems for hands-free telecommunication," *Speech Commun.*, vol. 20, no. 3, pp. 229–240, 1996.
[30] J. Benesty, J. Chen, and I. Cohen, *Design of Circular Differential Microphone Arrays*. Berlin, Germany: Springer-Verlag, 2015.
[31] G. Huang, J. Benesty, and J. Chen, "Subspace superdirective beamforming with uniform circular microphone arrays," in *Proc. IEEE Int. Workshop Acoust. Signal Enhancement*, pp. 1–5, 2016.
[32] S. Yan, "Optimal design of modal beamformers for circular arrays," *J. Acoust. Soc. Amer.*, vol. 138, no. 4, pp. 2140–2151, 2015.
[33] R. A. Monzingo and T. W. Miller, *Introduction to Adaptive Arrays*. Raleigh, NC, USA: SciTech, 1980.
[34] H. L. Van Trees, *Detection, Estimation, and Modulation Theory, Optimum Array Processing*. New York, NY, USA: Wiley, 2004.
[35] G. W. Elko, "Superdirectional microphone arrays," in *Acoustic Signal Processing for Telecommunication*. Berlin, Germany: Springer, 2000, pp. 181–237.
[36] L. L. Beranek, *Acoustics*. Woodbury, NY, USA: Acoust. Soc. Amer., 1986.
[37] M. Brandstein and D. Ward, *Microphone Arrays Signal Processing – Techniques and Applications*, Berlin, Germany: Springer-Verlag, 2001.
[38] J. Benesty, J. Chen, and C. Pan, *Fundamentals of Differential Beamforming*, Berlin, Germany: Springer-Verlag, 2016.
[39] L. Zhao, J. Benesty, and J. Chen, "Design of robust differential microphone arrays with the Jacobi–Anger expansion," *Appl. Acoust.*, vol. 110, pp. 194–206, 2016.
[40] M. Abramowitz and I. A. Stegun, *Handbook of Mathematical Functions with Formulas, Graphs, and Mathematical Tables*. New York, Ny, USA: Dover, 1970.
[41] R. M. Gray, *Toeplitz and Circulant Matrices: A Review* Boston-Delft: Now Publishers, Inc., 2006.
[42] B. Rafaely, *Fundamentals of Spherical Array Processing*. Berlin, Germany: Springer, 2015.
[43] D. Alon and B. Rafaely, "Beamforming with optimal aliasing cancellation in spherical microphone arrays," *IEEE/ACM Trans. Audio, Speech, Lang. Process.*, vol. 24, no. 1, pp. 196–210, Jan. 2016.
[44] J. Meyer, "Beamforming for a circular microphone array mounted on spherically shaped objects," *J. Acoust. Soc. Amer.*, vol. 109, pp. 185–193, 2001.
[45] S. C. Chan and H. H. Chen, "Uniform concentric circular arrays with frequency-invariant characteristics—Theory, design, adaptive beamforming and DOA estimation," *IEEE Trans. Signal Process.*, vol. 55, no. 1, pp. 165–177, Jan. 2007.

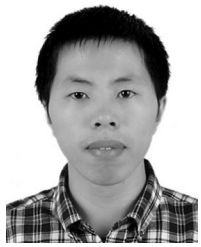

Gongping Huang (SM'13) received the Bachelor's degree in electronics and information engineering from the Northwestern Polytechnical University (NPU), Xi'an, China, in 2012, where he is currently working toward the Ph.D. degree in information and communication engineering. He is also a Visiting Ph.D. Student at Institut National de la Recherche Scientifique-Énergie, Matériaux et Télécommunications, University of Quebec, Montreal, QC, Canada. His research interests include microphone array signal processing, noise reduction, speech enhancement, and audio and speech signal processing.

Jacob Benesty was born in 1963. He received the Master's degree in microwaves from Pierre & Marie Curie University, Paris, France, in 1987, and the Ph.D. degree in control and signal processing from Orsay University, Orsay, France, in April 1991. During his Ph.D. (from November 1989 to April 1991), he worked on adaptive filters and fast algorithms at the Centre National d'Etudes des Telecomunications, Paris, France. From January 1994 to July 1995, he worked at Telecom Paris University on multichannel adaptive filters and acoustic echo cancellation. From October 1995 to May 2003, he was first a Consultant and then a Member of the Technical Staff at Bell Laboratories, Murray Hill, NJ, USA. In May 2003, he joined as a Professor the Institut National de la Recherche Scientifique-Énergie, Matériaux et Télécommunications, University of Quebec, Montreal, QC, Canada. He is also a Visiting Professor at the Technion, Haifa, Israel, an Adjunct Professor at Aalborg University, Denmark, and a Guest Professor at the Northwestern Polytechnical University, Xi'an, Shaanxi, China. In particular, he was the Lead Researcher at Bell Labs who conceived and designed the world-first real-time hands-free full-duplex stereophonic teleconferencing system. Also, he conceived and designed the world-first PC-based multiparty hands-free full-duplex stereoconferencing system over IP networks. He has invented many important technologies. His research interests include signal processing, acoustic signal processing, and multimedia communications.

He was the Co-chair of the 1999 International Workshop on Acoustic Echo and Noise Control and the General Cochair of the 2009 IEEE Workshop on Applications of Signal Processing to Audio and Acoustics. He received, with Morgan and Sondhi, the IEEE Signal Processing Society 2001 Best Paper Award, and, with Chen, Huang, and Doclo, the IEEE Signal Processing Society 2008 Best Paper Award, the Gheorghe Cartianu Award from the Romanian Academy in 2010, and the Best Paper Award from the IEEE WASPAA for a paper that he co-authored with Chen in 2011. He is also the Co-author of a paper for which Huang received the IEEE Signal Processing Society 2002 Young Author Best Paper Award.

Jingdong Chen (M'99–SM'09) received the Ph.D. degree in pattern recognition and intelligence control from the Chinese Academy of Sciences, Beijing, China, in 1998.

From 1998 to 1999, he was with ATR Interpreting Telecommunications Research Laboratories, Kyoto, Japan, where he conducted research on speech synthesis, speech analysis, as well as objective measurements for evaluating speech synthesis. He then joined the Griffith University, Brisbane, Australia, where he engaged in research on robust speech recognition and signal processing. From 2000 to 2001, he worked at ATR Spoken Language Translation Research Laboratories on robust speech recognition and speech enhancement. From 2001 to 2009, he was a Member of Technical Staff at Bell Laboratories, Murray Hill, NJ, USA, working on acoustic signal processing for telecommunications. He subsequently joined as a Chief Scientist WeVoice, Inc., Bridgewater, NJ, USA. He is currently a Professor at the Northwestern Polytechnical University, Xi'an, China. His research interests include acoustic signal processing, adaptive signal processing, speech enhancement, adaptive noise/echo control, microphone array signal processing, signal separation, and speech communication.

He served as an Associate Editor of the IEEE TRANSACTIONS ON AUDIO, SPEECH, AND LANGUAGE PROCESSING from 2008 to 2014. He is currently a Technical Committee (TC) Member of the IEEE Signal Processing Society (SPS) TC on Audio and Acoustic Signal Processing. He was the General Cochair of IWAENC 2016, the Technical Program Chair of IEEE TENCON 2013, a Technical Program Cochair of IEEE WASPAA 2009, IEEE ChinaSIP 2014, IEEE ICSPCC 2014, and IEEE ICSPCC 2015, and helped organize many other conferences. He co-authored the books *Fundamentals of Differential Beamforming* (Springer, 2016), *A Conceptual Framework for Noise Reduction* (Springer, 2015), *Design of Circular Differential Microphone Arrays* (Springer, 2015), *Study and Design of Differential Microphone Arrays* (Springer, 2013), *Speech Enhancement in the STFT Domain* (Springer, 2011), *Optimal Time-Domain Noise Reduction Filters: A Theoretical Study* (Springer, 2011), *Speech Enhancement in the Karhunen-Loève Expansion Domain* (Morgan & Claypool, 2011), *Noise Reduction in Speech Processing* (Springer, 2009), *Microphone Array Signal Processing* (Springer, 2008), and *Acoustic MIMO Signal Processing* (Springer, 2006). He is also a Co-editor/Co-author of the book *Speech Enhancement* (Springer, 2005).

Dr. Chen received the 2008 Best Paper Award from the IEEE Signal Processing Society (with Benesty, Huang, and Doclo), the Best Paper Award from the IEEE Workshop on Applications of Signal Processing to Audio and Acoustics in 2011 (with Benesty), the Bell Labs Role Model Teamwork Award twice, respectively, in 2009 and 2007, the NASA Tech Brief Award twice, respectively, in 2010 and 2009, the Japan Trust International Research Grant from the Japan Key Technology Center in 1998, and the Young Author Best Paper Award from the 5th National Conference on Man-Machine Speech Communications in 1998. He is also a co-author of a paper for which C. Pan received the IEEE R10 (Asia-Pacific Region) Distinguished Student Paper Award (First Prize) in 2016.